Supporting Information

Aggregation-state engineering and emission switching in D-A-D' AIEgens featuring dual emission, MCL and white electroluminescence

Ji-Hua Tan, Wen-Cheng Chen,* Shao-Fei Ni, Zhipeng Qiu, Yingying Zhan, Zhiwen Yang, Jingwen Xiong, Chen Cao, Yanping Huo* and Chun-Sing Lee*

1 Experimental Procedures

1.1 General information

All reactants and solvents used for the synthesis were commercially available and used without further purification unless otherwise specified. Elemental analyses were performed on a EuroVector EA3000 Organic Element Analyzer. Mass spectra were recorded by a 4800 Plus MALDI TOF/TOF Analyzer. ^{1}H and ^{13}C Nuclear Magnetic Resonance (NMR) spectra were recorded on a Bruker AVANCE III HD 400 MHz spectrometer. Thermogravimetric analysis (TGA) and differential scanning calorimetry (DSC) measurements were conducted under nitrogen atmosphere at a heating of rate 10 °C/min performed using a NETZSCH STA449F5 Jupiter Synchronous thermal analyzer. Cyclic voltammetry (CV) was measured on a CHI-660D electro-chemical workstation with three-electrode system, in which glassy carbon electrode, Pt wire electrode and Ag/AgCl electrode as working electrode, counter electrode and reference electrode, respectively. A solution of tetra-n-butylammonium hexafluorophosphate (Bu$_4$NPF$_6$) (0.1 M) in dichloromethane (DCM) was used as electrolyte. Highest occupied molecular orbital (HOMO) energy level was determined from the onset potential of oxidation by cyclic voltammetry, E_{HOMO}=-(E_{onset}+4.4); while lowest unoccupied molecular orbital (LUMO) energy level can be calculated using E_{HOMO} and optical band gap (E_g), E_{LUMO}=E_{HOMO}+E_g.[1] Ultraviolet–visible (UV–Vis) spectra were obtained using a Shimadzu, UV-2700 UV-Vis spectrophotometer. Both steady-state, time-resolved photoluminescence (PL) spectra and transient decay spectra at 77 K and 300 K were collected from an Edinburgh FLS 980 spectrophotometer, which equipped with Oxford Instruments nitrogen cryostat (Optistat DN) for temperature control. Raman spectra were recorded by a Renishaw inVia Raman Microscope with 785 nm excitation. Powder X-Ray Diffraction (PXRD) experiments were performed on a BRUKER D8 ADVANCE X-ray diffractometer at a scan rate of 10° (2 Theta) per min.

Synthesis of compound CTM and tCTM
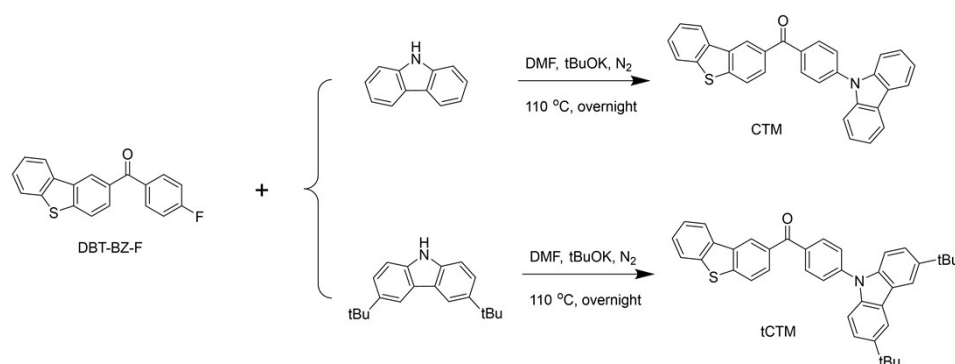
Scheme S1 Synthesis route of **CTM** and **tCTM**.

Dibenzo[*b,d*] thiophen-2-yl (4-fluorophenyl) methanone (**DBT-BZ-F**) was synthesized according to the previous work.[2] The synthesis route of presented molecular are shown in **Scheme S1**.

Procedure for the synthesis of (4-(9*H*-carbazol-9-yl) phenyl) (dibenzo [*b,d*] thiophen-2-yl) methanone (CTM)

To a mixture of **DBT-BZ-F** (612.1 mg, 2 mmol) and 9*H*-carbazole (417.7 mg, 2.5 mmol) in dry *N, N*-Dimethylformamide (DMF, 20mL), *t*-BuOK powder (448.8 mg, 4 mmol) was added after the reaction system was evacuated under vacuum and purged with dry nitrogen for three times. The mixture was under stirring and heated under reflux overnight. After the mixture was cooled, it was subsequently poured into deionized water (400 mL) and stirred for 5 minutes. Organic layer was extracted with dichloromethane for three times, gathered and washed with brine twice, then dried over anhydrous $MgSO_4$. Residue was obtained after solvent evaporation under reduced pressure, and to give **CTM** as white powder after purifying by silica-gel column chromatography using dichloromethane/petroleum as eluent. Yield: 82%; ^{1}H NMR (400 MHz, $CDCl_3$) δ ppm: 8.71 (s, 1H), 8.28-8.24 (m, 1H), 8.14 (dd, J = 14.8, 8.1 Hz, 4H), 8.00 (s, 2H), 7.94-7.88 (m, 1H), 7.80-7.75 (m, 2H), 7.59-7.50 (m, 4H), 7.46 (t, J = 7.7 Hz, 2H), 7.33 (td, J = 7.5, 7.1, 1.0 Hz, 2H); ^{13}C NMR (101 MHz, $CDCl_3$) δ ppm: 195.37, 144.33, 141.68, 140.29, 139.78, 136.38, 135.64, 135.15, 133.81, 131.90, 128.12, 127.55, 126.38, 126.24, 124.98, 123.87, 123.56, 123.01, 122.72, 122.07, 120.63, 120.50, 109.83; MALDI-TOF-MS m/z: 453.1554. Elemental analyses (%) calcd for $C_{31}H_{19}NOS$: C 82.09, H 4.22, N 3.09, O 3.53, S 7.07; found:C 82.16, H 4.18, N 3.15, O 3.56, S 6.96.

Procedure for the synthesis of (4-(3, 6-di-*tert*-butyl-9*H*-carbazol-9-yl) phenyl) (dibenzo [*b,d*] thiophen-2-yl) methanone (tCTM)

The synthesis of **tCTM** is similar to that of **CTM**, except for the aromatic amine 3, 6-di-*tert*-butyl-9*H*-carbazole. The residue was purified by silica-gel column chromatography using dichloromethane/petroleum as eluent, and to give **tCTM** as yellowish-white powder. Yield: 85%; ^{1}H NMR (400 MHz, $CDCl_3$) δ ppm: 8.71 (d, J = 1.1 Hz, 1H), 8.28-8.23 (m, 1H), 8.16 (d, J = 1.4 Hz, 2H), 8.13-8.08 (m, 2H), 8.00 (d, J = 1.1 Hz, 2H), 7.90 (dt, J = 5.3, 3.1 Hz, 1H), 7.79-7.73 (m, 2H), 7.55-7.48 (m, 6H), 1.48 (s, 18H); ^{13}C NMR (101 MHz, $CDCl_3$) δ ppm: 195.44, 144.22, 143.68, 142.25, 139.78, 138.60, 135.78, 135.61, 135.17, 133.94, 131.88, 128.12, 127.52, 125.80, 124.97, 123.93, 123.90, 123.56, 123.00, 122.70, 122.08, 116.44, 109.34, 34.81, 32.00; MALDI-TOF-MS m/z: 565.3025. Elemental analyses (%) calcd for $C_{39}H_{35}NOS$: C 82.79, H 6.24, N 2.48, O 2.83, S 5.67; found: C 82.86, H 6.21, N 2.52, O 2.78, S 5.66.

1.2 Single crystal X-ray crystallography

Single crystal of **CTM-B** and **tCTM-B** were obtained by slow diffusion of poor solvent *n*-hexane to tetrahydrofuran in a sealed test tube, while **CTM-W** and **tCTM-W** yielded from

slow evaporation of dichloromethane and methanol solution at room temperature. Single crystal diffraction data was collected from the instrument SuperNova, Dual, Cu at zero, AtlasS2 diffractometer with Cu-Kα radiation (λ=1.54184 Å) or Mo-Kα radiation (λ=0.71073 Å) at the temperature of 100.00 (10) K. The corresponding CCDC reference number (CCDC: 1975024-1975027) and the data can be obtained free of charge from The Cambridge Crystallographic Data Centre via www.ccdc.cam.ac.uk/data_request/cif. Their crystal data are listed on **Table S3**.

1.3 Theoretical calculations

The ground state (S_0) geometries include of isolated molecules (monomers) and adjacent molecules (dimers) were extracted from single crystal structures. Based on S_0 geometries, vertical transition energy were calculated in B3LYP/6-31 G* level [3] via time-dependent density functional theory (TD-DFT), using Gaussian 09 program package.[4] Spin-orbital couplings (SOC) matrix elements were calculated in the same level as mentioned, via Orca package.[5]

1.4 Device fabrication and measurement

Synthetic materials were used in devices fabrication after sublimation, while other materials used as auxiliary layers were commercially available and used without further purification. ITO-coated glass substrates with a sheet resistance of 15 Ω sqrt^{-1} were used as a transparent anode, which were washed using detergent and underwent ultrasound bath of deionized water, acetone and isopropanol, successively for 15 minutes. And used after thoroughly dried and treated with O_2 plasma for half of an hour. Under high vacuum better than 10^{-6} Torr, materials were heated to sublimate and deposited onto ITO substrates. The rates of deposition were detected and controlled via quartz crystal oscillators, maintaining 1~2 Å/s for organic materials, 0.1 Å/s for ~LiF and ~5 Å/s for aluminum cathode, respectively. Electroluminescence (EL) spectra and luminance were collected by a Spectroradiometer (Photo Research PR 650) and PMA-12 photonic multichannel analyzer (Hamamatsu), respectively. Current density and voltage were recorded on a Keithley 237 power source (Tektronix). External quantum efficiencies of devices were calculated using EL spectra and current, assuming the devices were Lambertian light sources.
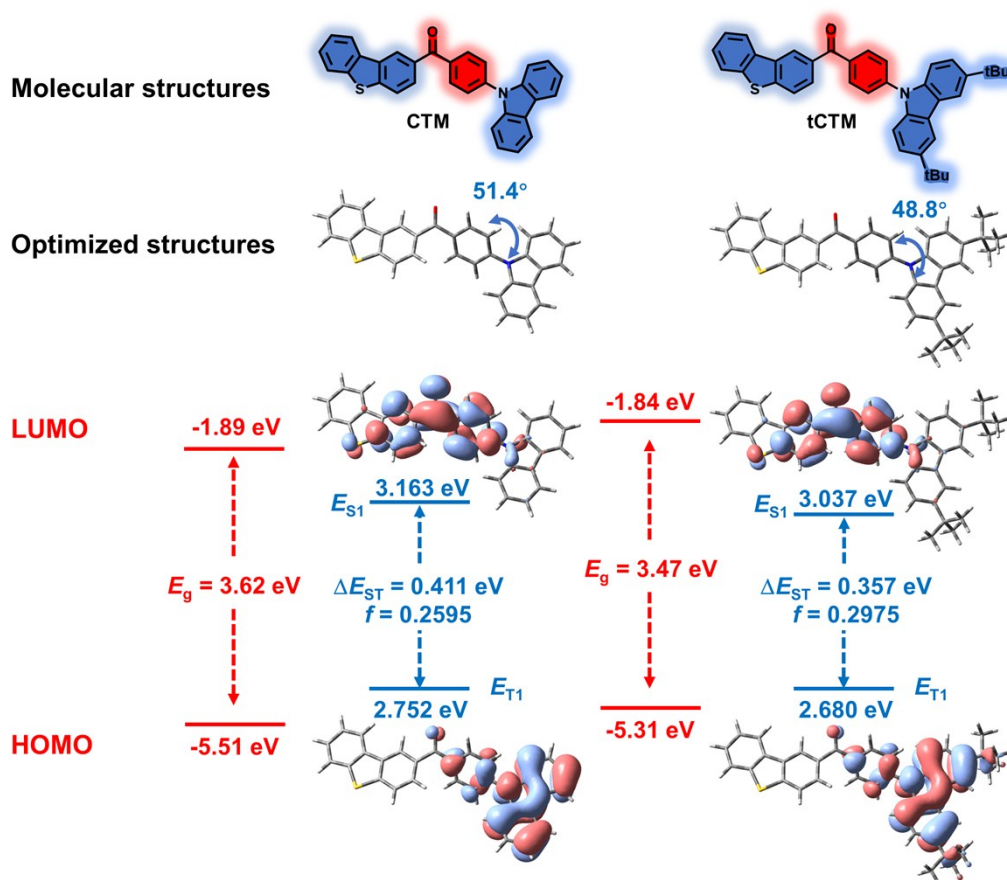
2. Results and Discussion

Fig. S1 Molecular structures, optimized ground-state (S_0) structures, HOMO and LUMO distributions, and energy levels of HOMOs/LUMOs, energy gap (E_g) of **CTM** and **tCTM** based on DFT at the B3LYP/6-31G* level. Calculated energy levels of first singlet (S_1) state (E_{S1}) and first triplet (T_1) state (E_{T1}), splitting energies of S_1 and T_1 (ΔE_{ST}), and oscillator strength (f) of **CTM** and **tCTM** based on TD-DFT at the same level are listed.
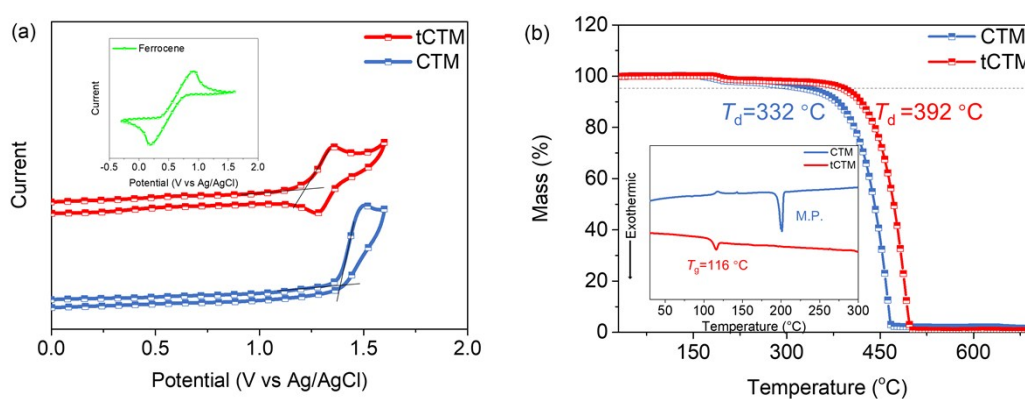
Fig. S2. (a) Cyclic voltammetry (CV) and (b) TGA (inset: DSC) curves of **CTM** and **tCTM.**

2.1 Photoluminescent properties
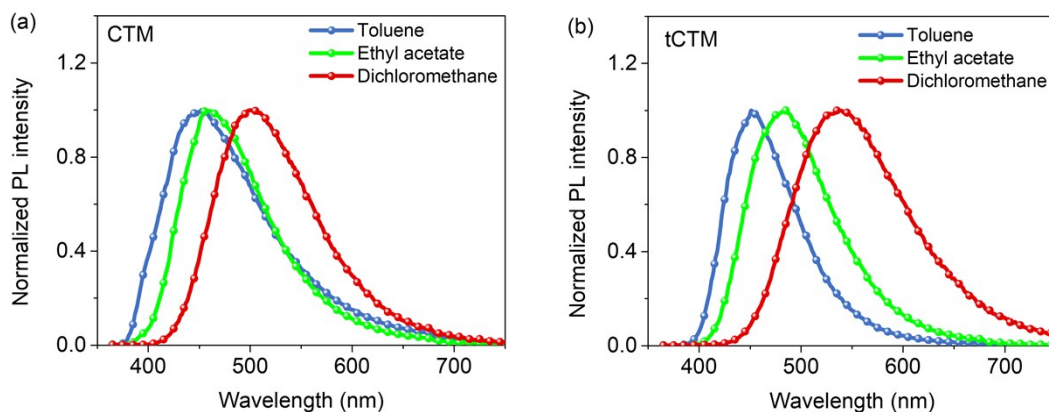
Fig. S3. PL spectra of (a) **CTM** and (b) **tCTM** in different solvents (10μM) with increased polarity.

Table S1 Summary photophysical data of **CTM** and **tCTM**.

Compound	λ_{abs}[a] [nm]	λ_{em}[a] [nm]	τ_d[b] [μs]	Φ_{PL}[c] [%]	E_S/E_T[d] [eV]	ΔE_{ST}[e] [eV]	HOMO/LUMO[f] [eV]	T_d[g] [°C]	T_g [°C]
CTM	292/ 340	404/ 430	0.6/ 2.4	23.6/ 30.4	3.069/ 2.838	0.262	-5.75/-2.73	332	N.D. [h]
tCTM	296/ 349	476	0.1/ 4.0	38.7/ 45.2	3.013/2.7 49	0.264	-5.60/-2.69	392	116

[a]Measured in Tetrahydrofuran (THF) solution (10 μM) at 300 K. [b]Lifetimes of delay fluorescence measured in DCM solution (10 μM) before/after N$_2$ bubbling for 30 min at 300 K. [c]Absolute photoluminescence quantum yield measured in DCM solution (10 μM) before/after N$_2$ bubbling for 30 min with an integrating sphere at 300 K. [d]E_S and E_T were obtained from the onsets of fluorescence spectra and the shortest-wavelength local excited (LE) peak in phosphorescence spectra respectively for two emitters in 2-Methyl-THF solution (10 μM) at 77 K. [e]$\Delta E_{ST}=E_S-E_T$. [f]E_{HOMO} was determined from the half-wave potentials of the oxidation reduction curves. $E_{LUMO}=E_{HOMO}+E_g$; E_g was obtained from the onsets of UV/Vis absorption spectra. [g] corresponding to 5% weight loss. [h] Not detected within the measured temperature range.
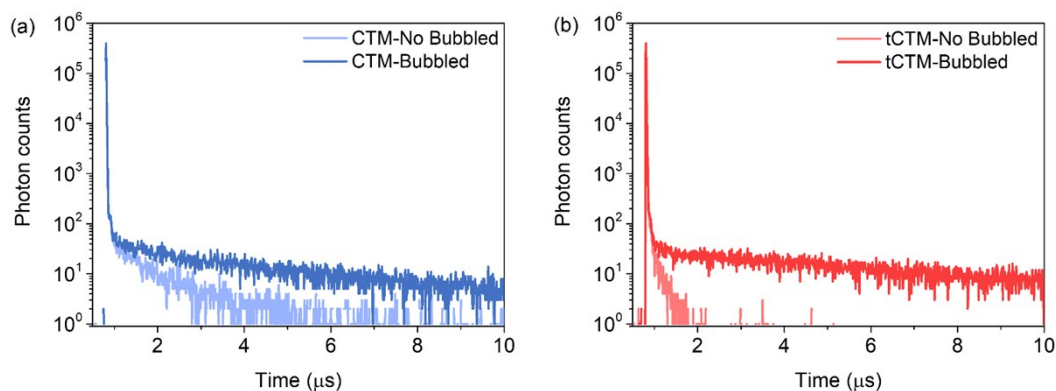
Fig. S4 Comparison of no N_2 bubbled and N_2 bubbled transient PL decays of (a) **CTM** and (b) **tCTM** in diluted DCM solutions (10 µM) at 300 K; λ_{ex}=375 nm.
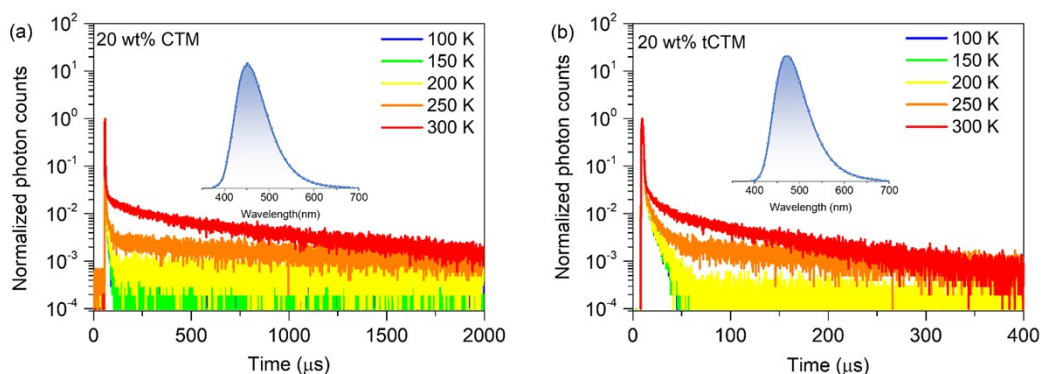

Fig. S5 Temperature-dependent transient PL decay curves of (a) **CTM** and (b) **tCTM** doped films (20 wt% doped into **DPEPO**) from 100 K to 300 K; insets: normalized PL spectra at 300 K, λ_{ex}=350 nm.
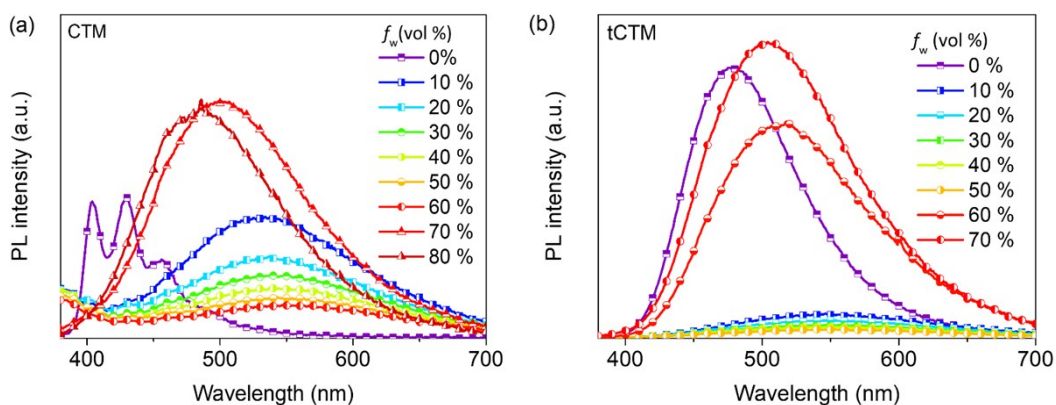

Fig. S6 PL spectra of (a) **CTM** and (b) **tCTM** (100 µM) in THF/water mixtures with various water fractions (f_w); λ_{ex}=350 nm.
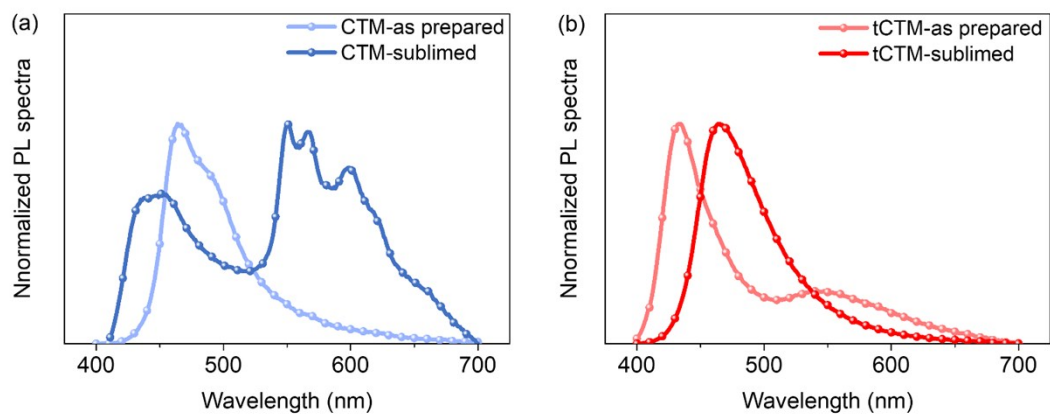
Fig. S7 Normalized PL spectra of (a) **CTM** and (b) **tCTM** at different aggregated states under ambient conditions; λ_{ex}=350 nm.
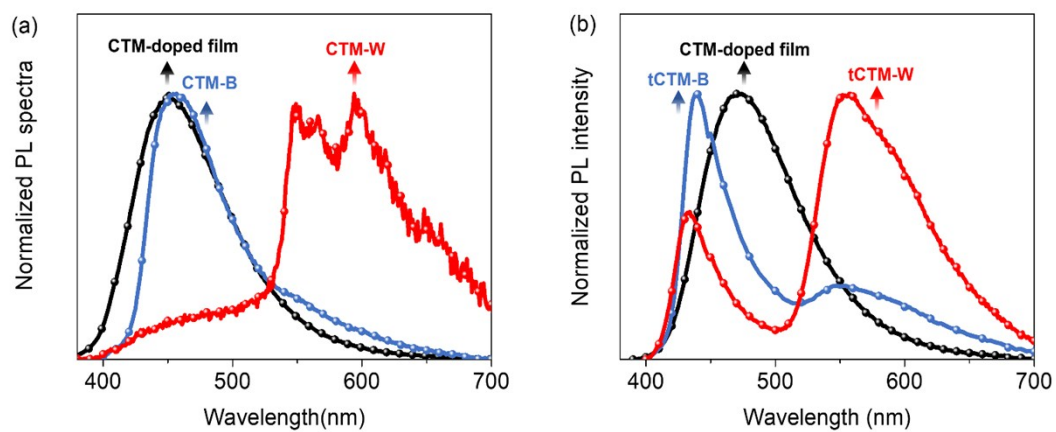

Fig. S8 Normalized PL spectra of (a) **CTM** and (b) **tCTM** doped films (20 wt% doped into **DPEPO**) and single crystals, λ_{ex}=350 nm.
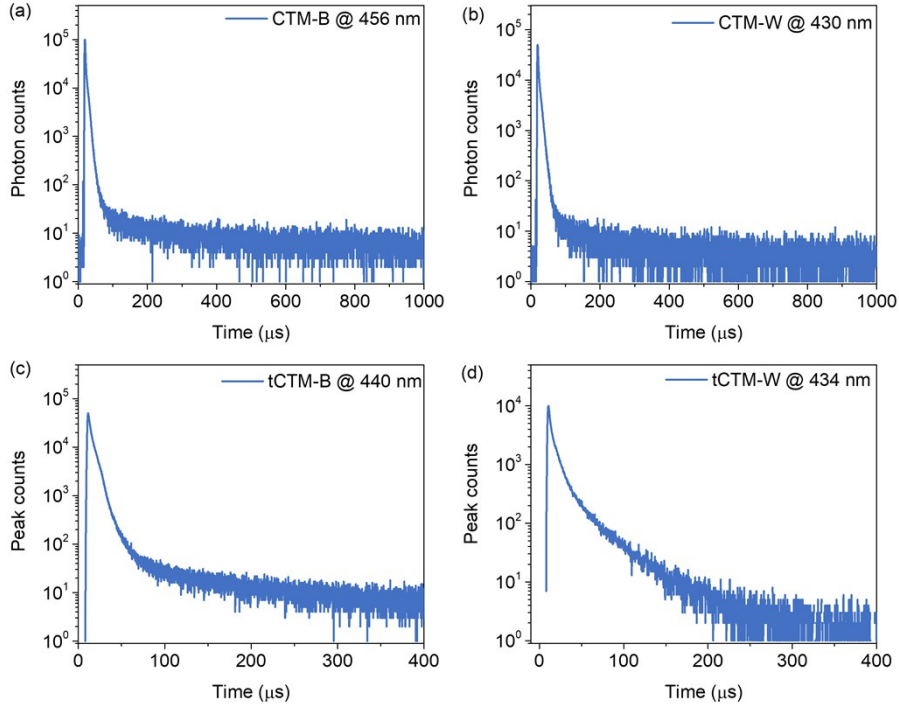
Fig. S9 Transient PL decay curves of single crystals (a) **CTM-B**, (b) **CTM-W**, (c) **tCTM-B** and (d) **tCTM-W**, respectively at 300 K under vacuum condition; λ_{ex}=350 nm.
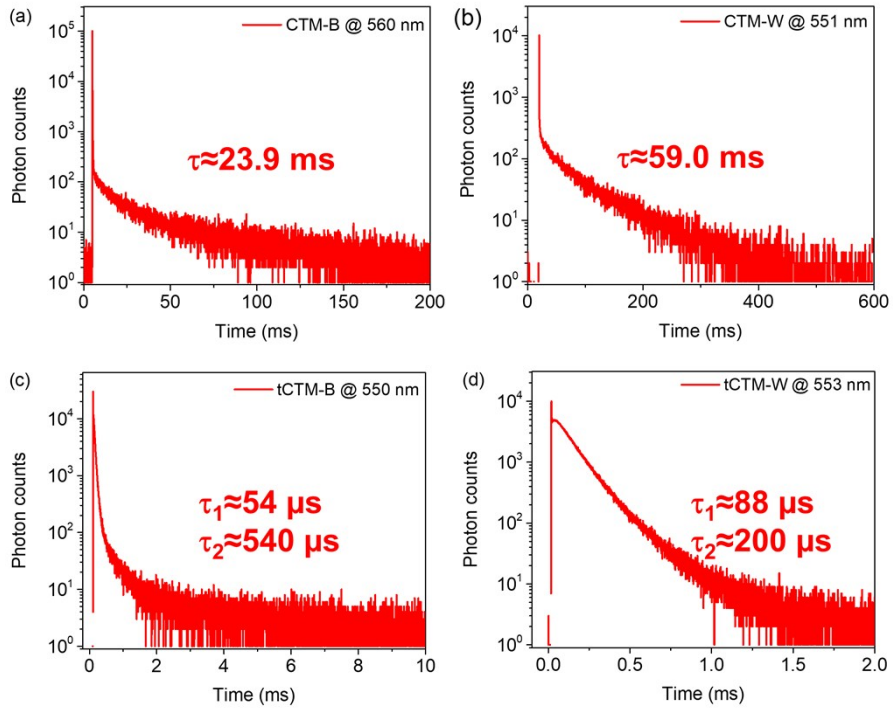

Fig. S10 Transient PL decay curves of single crystals (a) **CTM-B**, (b) **CTM-W**, (c) **tCTM-B** and (d) **tCTM-W**, respectively at 300 K under vacuum condition; λ_{ex}=350 nm.

Table S2 Summary photophysical data of crystal **CTM-B**, **CTM-W**, **tCTM-B** and **tCTM-W**.

| Crystal | @ 300 K (Vacuum) | | | @ 77 K (N$_2$) | | |
| | $\lambda_{em\text{-}blue}$ | $\lambda_{em\text{-}orange}$ | τ_{orange} | $\lambda_{em\text{-}blue}$ | $\lambda_{em\text{-}orange}$ | ΔE_{ST}[e] |
	[nm]	[nm]	[ms] (%)	[nm]	[nm]	[eV]
CTM-B	456	560[a]	23.9	444	484 [d]/535	0.23
CTM-W	430	551	59.0	430	482/544	0.30
tCTM-B	440	550	0.054 (65.6)[c]/0.54 (34.34)[d]	440	462/542	0.14
tCTM-W	434	553	0.088 (91.57)[c]/0.2 (8.43)[d]	437	454/530	0.11

[a] Delayed 0.1 ms. Lifetimes and the corresponding contributions of [b] τ_1 and [c] τ_2 of biexponential decays at orange component. [d] Delayed 5 ms. [e] ΔE_{ST} of monomer, determined from monomeric fluorescence and phosphorescent at 77 K.
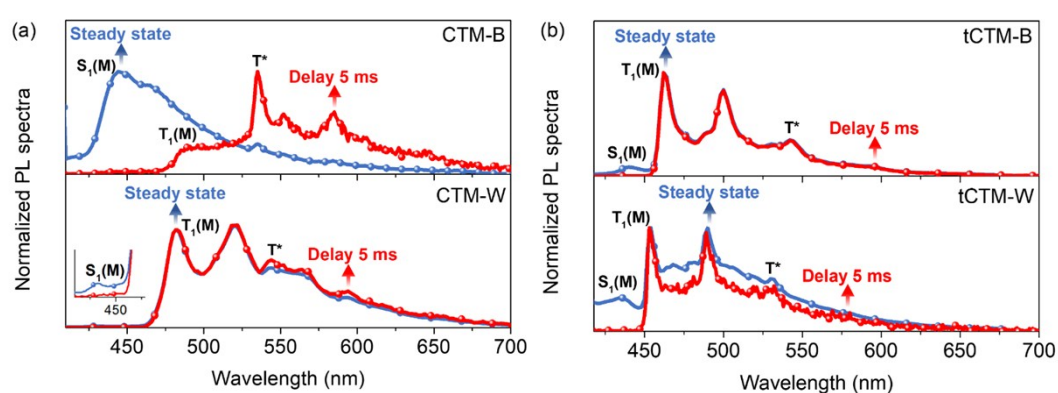

Fig. S11 Normalized TRPL spectra of (a) **CTM-B**, **CTM-W**; and (b) **tCTM-B**, **tCTM-W**, respectively at 77 K under nitrogen atmosphere; λ_{ex}=350 nm. S$_1$(M), T$_1$(M) represent the first singlet excited states and triplet excited states of monomers in crystals. While T* represents the triplet excited state of intermolecular electronic coupling dimer in crystals.

2.2 Single crystal analysis

Table S3 Summary of the crystal data for **CTM-B**, **CTM-W**, **tCTM-B** and **tCTM-W**.

| Identification code	CTM-B	CTM-W	tCTM-B	tCTM-W
Empirical formula	$C_{31}H_{19}NOS$	$C_{31}H_{19}NOS$	$C_{39}H_{35}NOS$	$C_{39}H_{35}NOS$
CCDC number	1975024	1975025	1975026	1975027
Formula weight	453.53	453.53	565.74	565.74
Temperature / K	100.00 (10)	100.00 (10)	100.00 (10)	100.00 (10)
Crystal system	monoclinic	monoclinic	monoclinic	monoclinic
Space group	$P2_1/n$	$P2_1/c$	$P2_1/c$	$P2_1/n$
a/Å	9.6739 (2)	16.7886 (5)	16.7257 (10)	21.700 (2)
b/Å	8.3766 (2)	32.6553 (9)	12.0845 (5)	6.7601 (5)
c/Å	27.1700 (6)	8.0391 (2)	15.9769 (9)	22.202 (2)
$\alpha/°$	90	90	90	90
$\beta/°$	92.264 (2)	97.373 (3)	114.206 (7)	109.472 (12)
$\gamma/°$	90	90	90	90
Volume/Å^3	2199.97 (9)	4370.9 (2)	2945.3 (3)	3070.7 (6)
Z	4	8	4	4
$\rho_{calc}g/cm^3$	1.369	1.378	1.276	1.224
μ/mm^{-1}	1.499	1.509	0.143	1.169
F (000)	944.0	1888.0	1200.0	1200.0
Crystal size/mm^3	0.12×0.11×0.1	0.13 × 0.12 × 0.1	0.14 × 0.12 × 0.11	0.13 × 0.12 × 0.11
Radiation	CuKα (λ = 1.54184)	CuKα (λ = 1.54184)	MoKα (λ = 0.71073)	CuKα (λ = 1.54184)
2Θ range for data collection/°	6.512 to 146.914	5.308 to 147.192	4.3 to 49.994	4.932 to 149.304
Index ranges	$-11 \leq h \leq 10, -6 \leq k \leq 10, -33 \leq l \leq 32$	$-20 \leq h \leq 18, -38 \leq k \leq 40, -6 \leq l \leq 9$	$-19 \leq h \leq 15, -14 \leq k \leq 14, -15 \leq l \leq 18$	$-26 \leq h \leq 18, -8 \leq k \leq 5, -27 \leq l \leq 27$
Reflections collected	7850	18374	13420	11347
Independent reflections	4292 [R_{int} = 0.0201, R_{sigma} = 0.0263]	8592 [R_{int} = 0.0357, R_{sigma} = 0.0455]	5195 [R_{int} = 0.0340, R_{sigma} = 0.0438]	6048 [R_{int} = 0.0537, R_{sigma} = 0.0731]
Data/restraints/parameters	4292/0/307	8592/14/613	5195/14/385	6048/0/385
Goodness-of-fit on F^2	1.070	1.056	1.042	1.033
Final R indexes [I>=2σ (I)]	R_1 = 0.0481, wR_2 = 0.1260	R_1 = 0.0828, wR_2 = 0.1856	R_1 = 0.0526, wR_2 = 0.1191	R_1 = 0.0905, wR_2 = 0.2287
Final R indexes [all data]	R_1 = 0.0534, wR_2 = 0.1302	R_1 = 0.1064, wR_2 = 0.2103	R_1 = 0.0634, wR_2 = 0.1261	R_1 = 0.1282, wR_2 = 0.2658
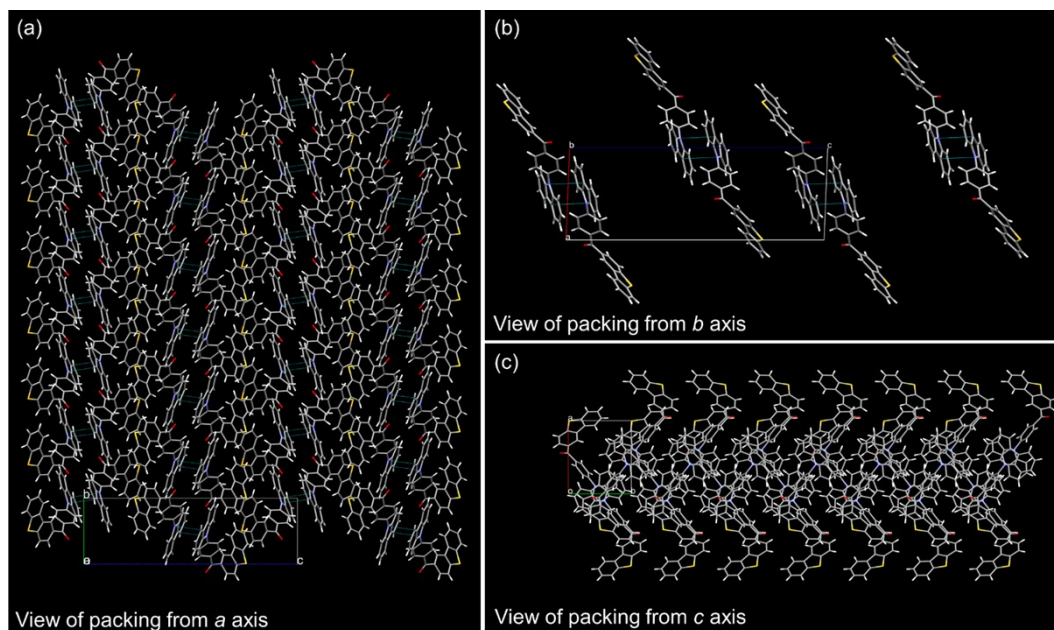
Fig. S12 Views of molecular packing of single crystal **CTM-B** from (a) *a* axis, (b) *b* axis and (c) *c* axis, respectively; blue lines indicate the π–π interactions from the **Cz** groups on the neighboring molecules.
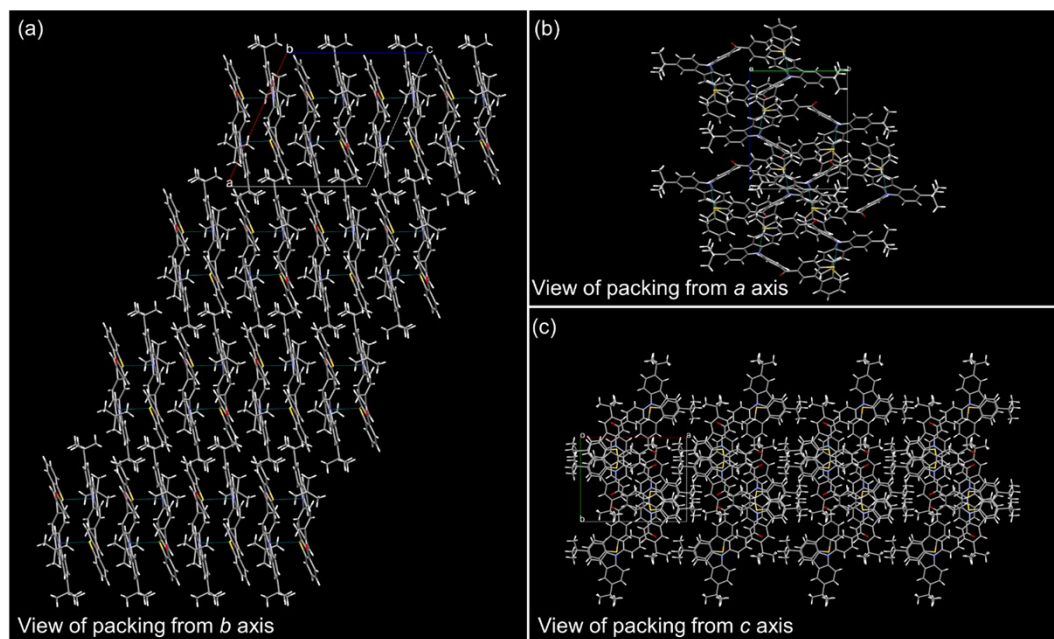

Fig. S13 Views of molecular packing of **tCTM-B** from (a) *b* axis, (b) *a* axis and (c) *c* axis, respectively; blue lines represent the N⋯S intermolecular interactions.
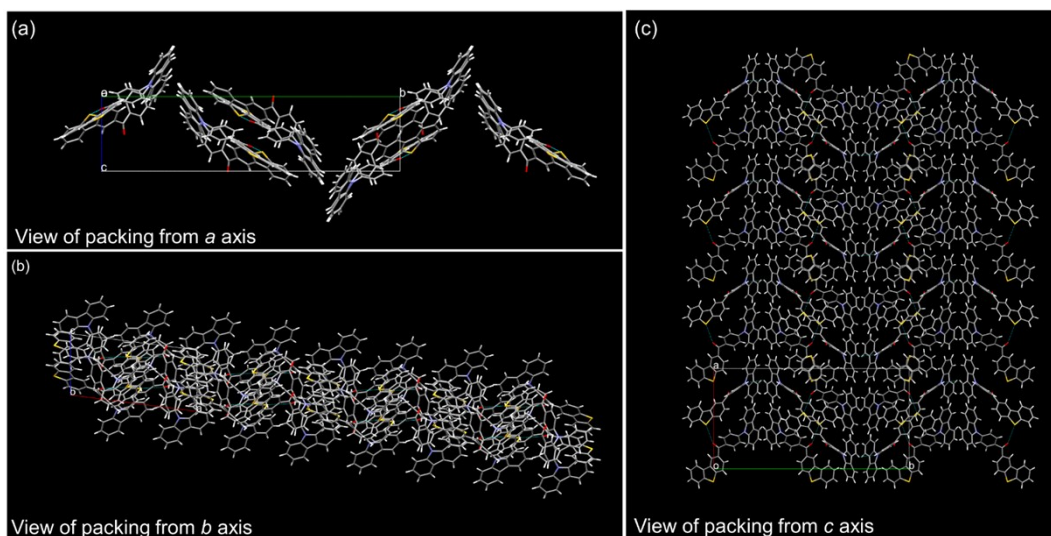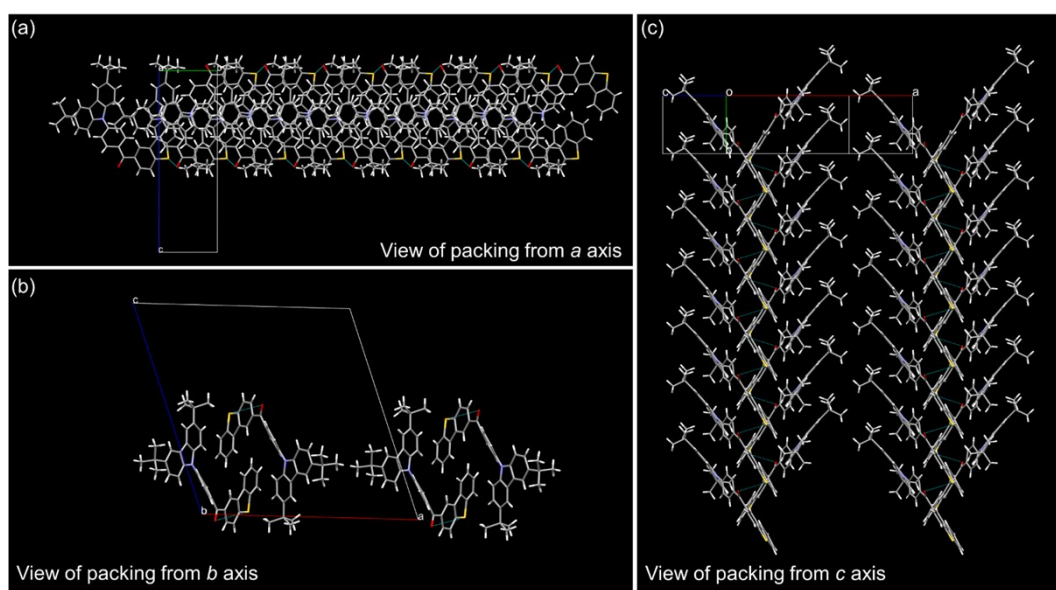
Fig. S14 Views of molecular packing of **CTM-W** from (a) *a* axis, (b) *b* axis and (c) *c* axis; respectively, blue lines represent the C=O···S intermolecular interactions.

Fig. S15 Views of molecular packing of **tCTM-W** from (a) *a* axis, (b) *b* axis and (c) *c* axis, respectively; blue lines represent the C=O···S intermolecular interactions.
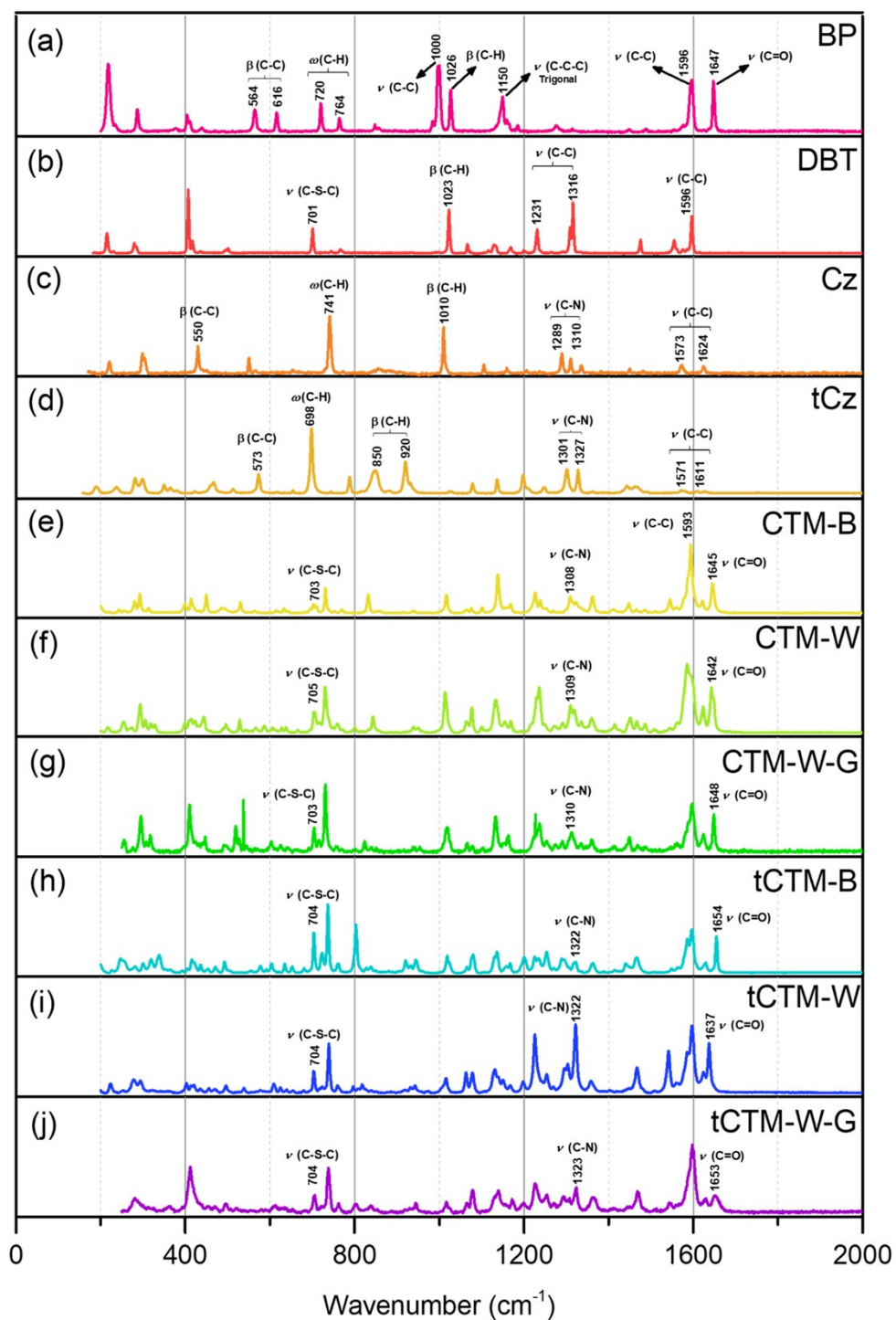
2.3 Raman spectra analysis

Fig. S16 Raman spectra of (a) **BP**, (b) **DBT**, (c) **Cz**, (d) **tCz**, (e) **CTM-B**, (f) **CTM-W**), (g) **CTM-W-G** (ground sample), (h) **tCTM-B,** (i) **tCTM-W**, and (j) **tCTM-W-G** (ground sample); ν represents stretching; β represents in-plane bending; ω represents out-of-plane bending.
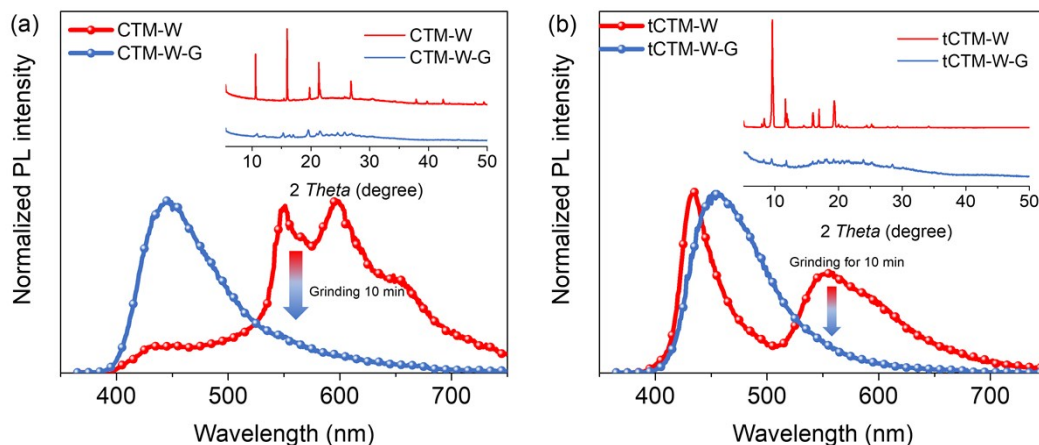
14

Fig. S17 Normalized PL spectra of crystal and ground sample (a) **CTM-W** and **CTM-W-G**, (b) **tCTM-W** and **tCTM-W-G**. Insets: corresponding PXRD patterns of crystals and ground samples. Completely grinding for 10 min. λ_{ex}=350 nm.

2.4 Theoretical calculations

Table S4 Theoretical-calculation results of **CTM-B**, **CTM-W**, **tCTM-B**, and **tCTM-W**.

Parameters	CTM-B		CTM-W		tCTM-B		tCTM-W	
	Monomer	Dimer	Monomer	Dimer	Monomer	Dimer	Monomer	Dimer
E_{S1} [eV]	3.19	3.20	3.19	3.16	3.05	2.98	3.07	3.07
E_{T1} [eV]	2.90	2.82	2.79	2.80	2.72	2.70	2.73	2.74
ΔE_{ST} [eV]	0.29	0.38	0.40	0.36	0.33	0.28	0.34	0.33
$\zeta S_1 T_1$[a] [cm^{-1}]	0.75	0.01	0.75	0.70	0.65	0.59	0.63	0.64
$\zeta S_1 T_2$[b] [cm^{-1}]	1.17	0.79	1.08	0.25	1.47	0.13	1.48	0.19
$\zeta S_1 T_3$[c] [cm^{-1}]	2.91	0.00	2.90	0.96	0.36	0.09	0.43	1.46

[a] SOC matrix elements between S_1 state and T_1 state. [b] SOC matrix elements between S_1 state and T_2 state. [c] SOC matrix elements between S_1 state and T_3 state.

Table S5 The electrical density contour of HOMO-1, HOMO, LUMO and LUMO+1, of dimers of **CTM-W** and **tCTM-W** based on TD-DFT results.
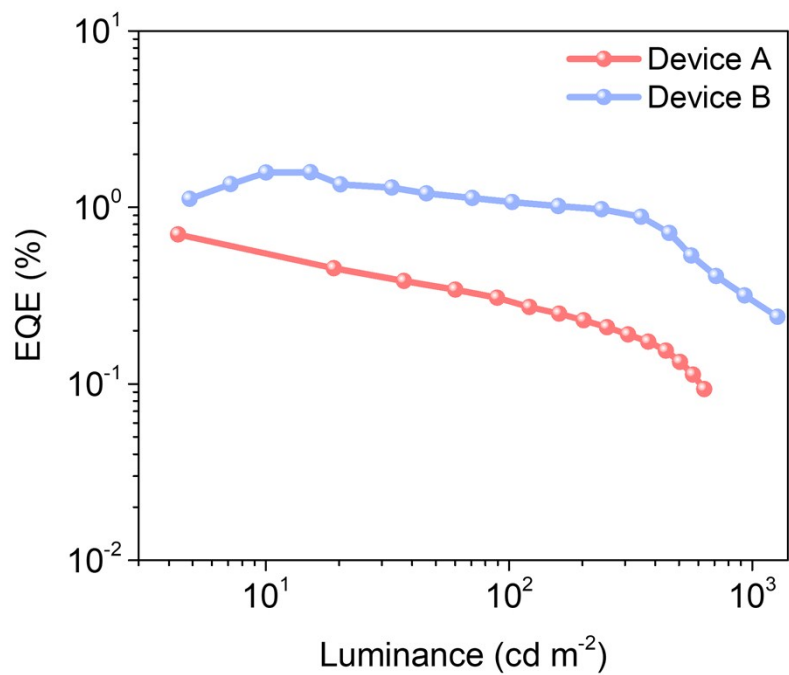
	CTM-W	tCTM-W
LUMO+1		
LUMO		
HOMO		
HOMO-1		
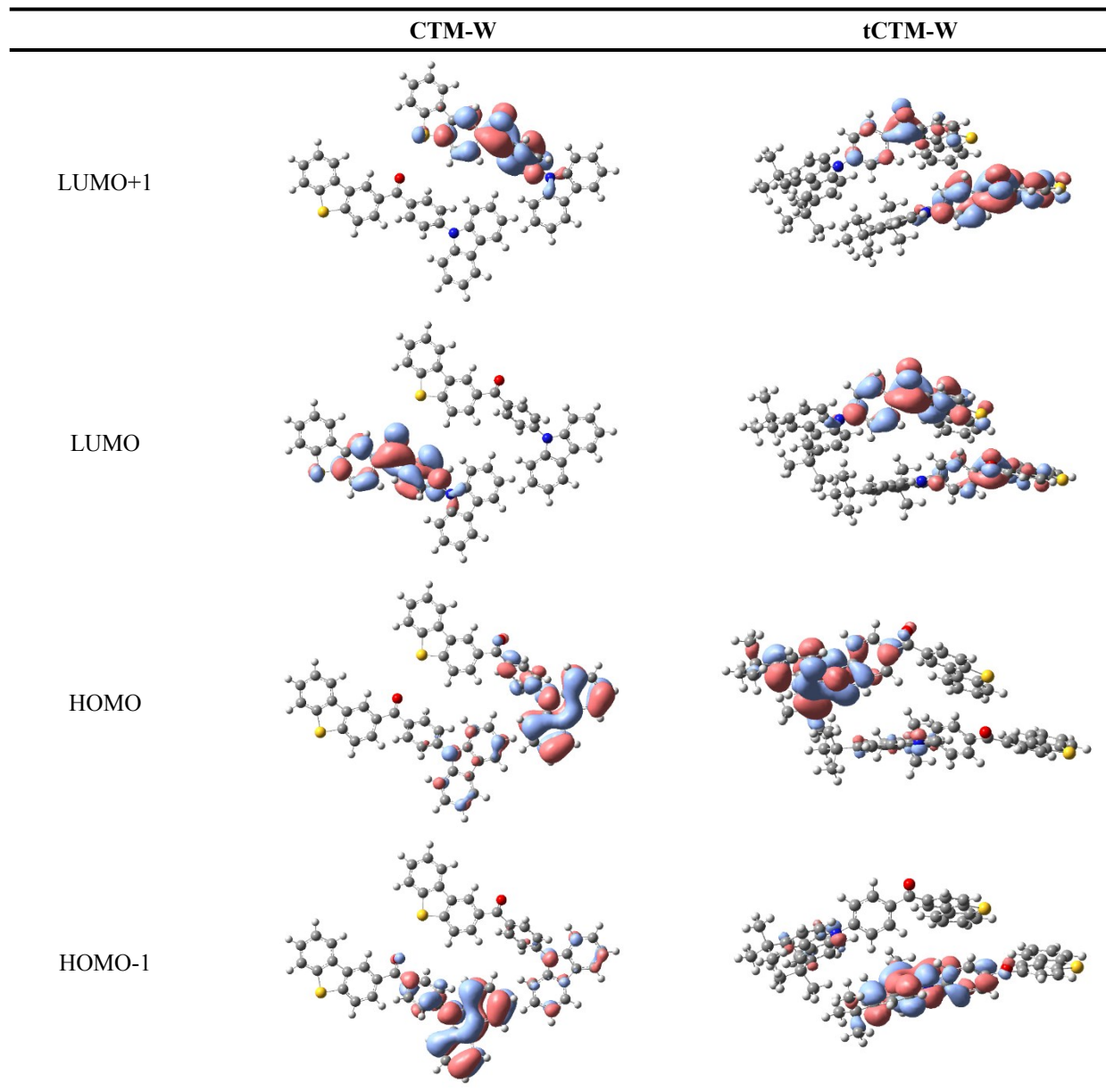
Fig. S18 EQE–luminance curve of device A and device B.
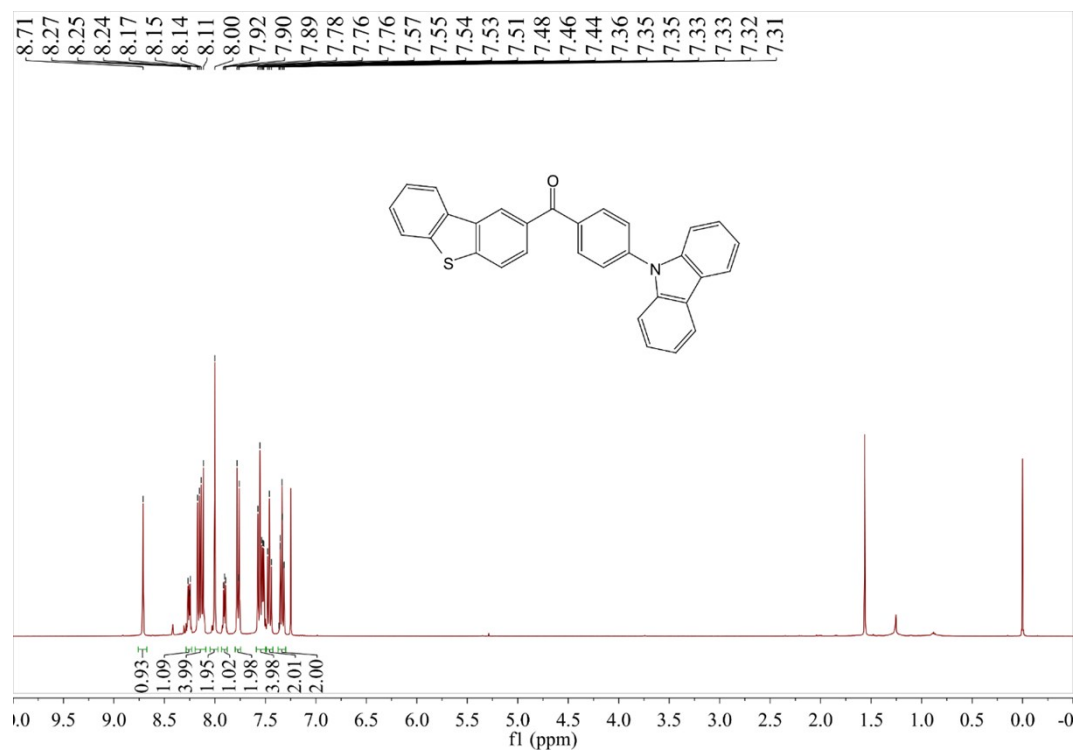
Fig. S19 ^{1}H NMR spectrum of compound **CTM** measured in CDCl₃.

17
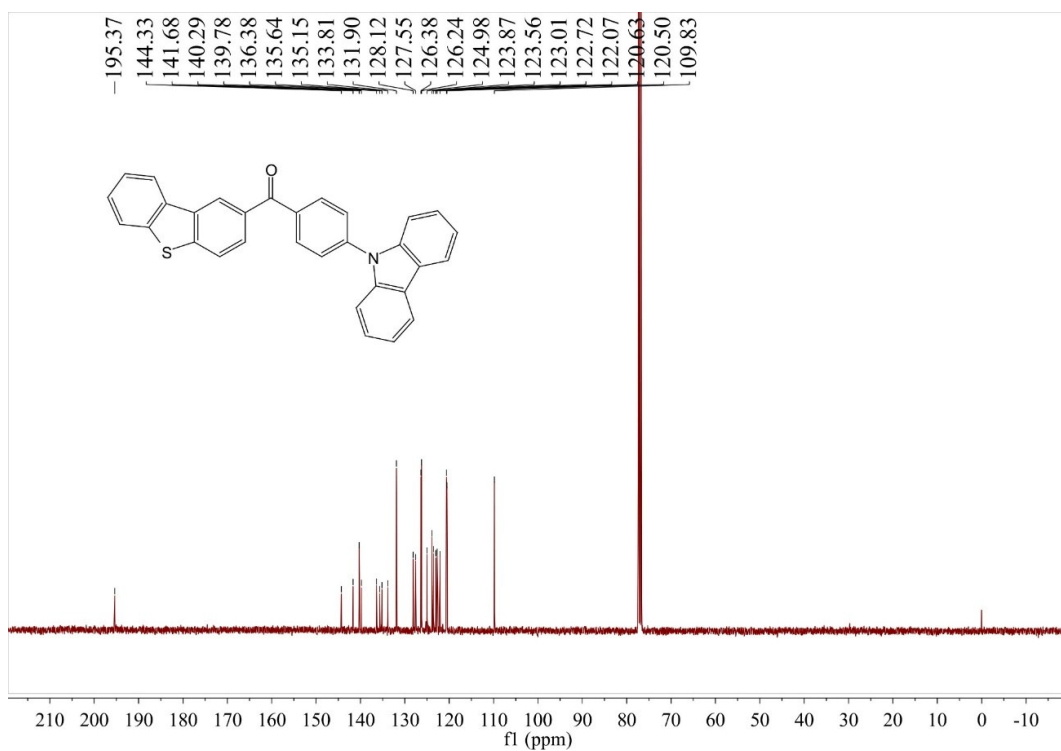
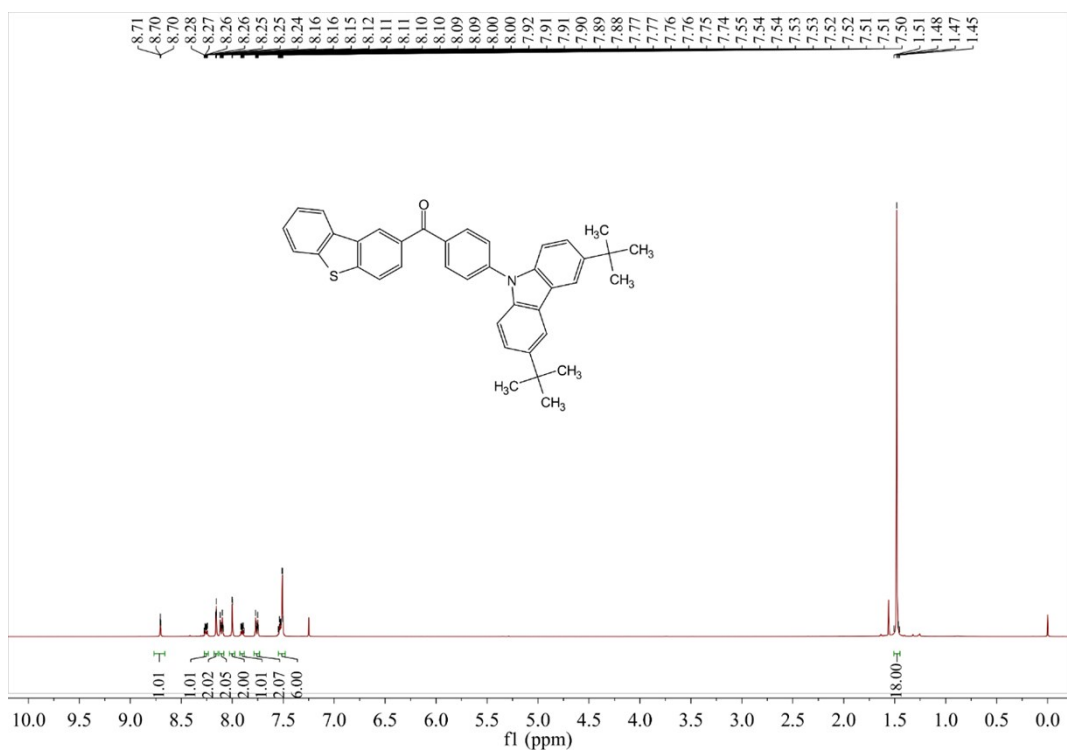**Fig. S20** ^{13}C NMR spectrum of compound **CTM** measured in CDCl$_3$.

Fig. S21 ^{1}H NMR spectrum of compound **tCTM** measured in CDCl$_3$.
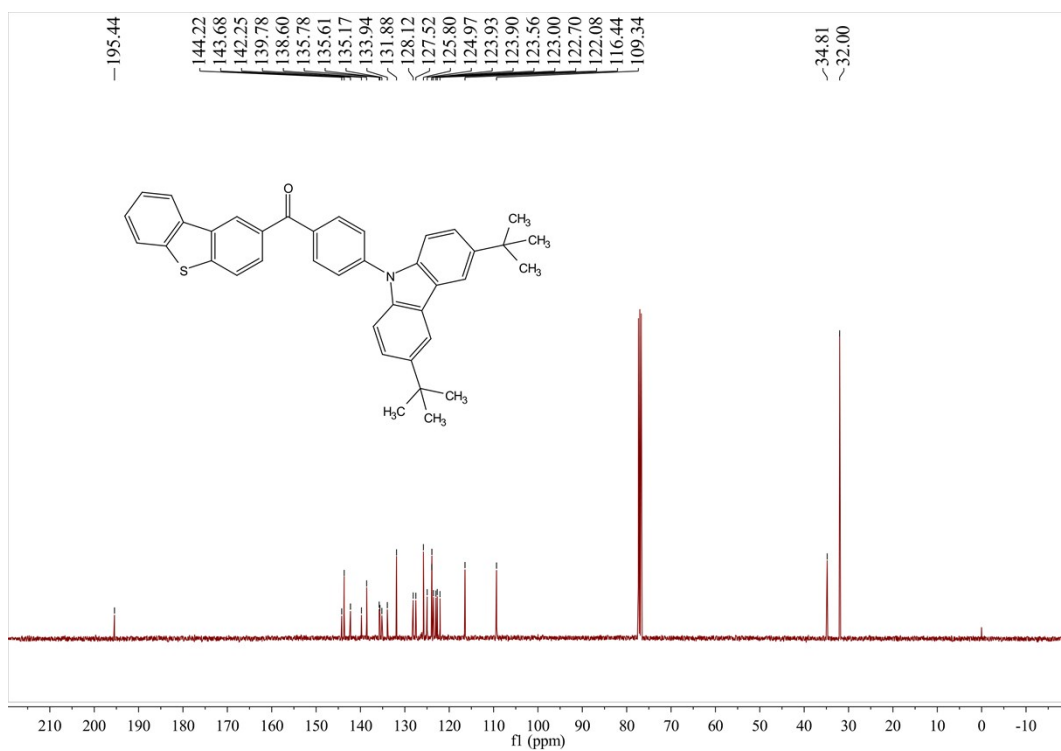
18

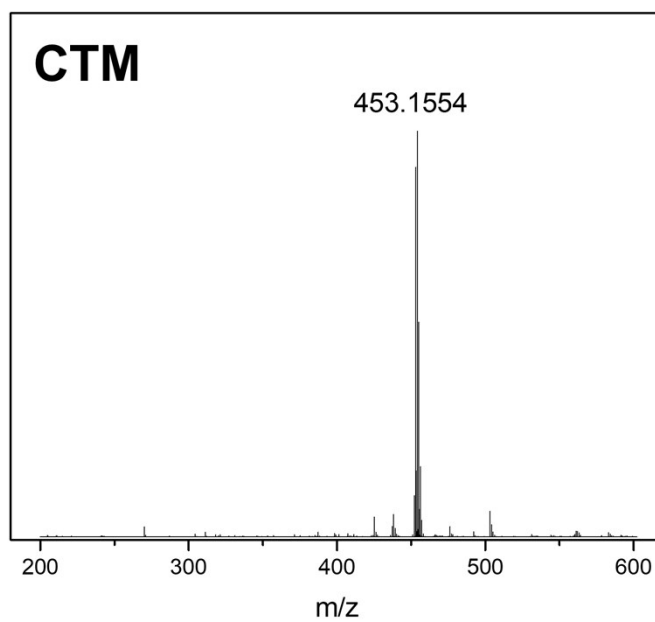**Fig. S22** ^{13}C NMR spectra of compound **tCTM** measured in CDCl$_3$.

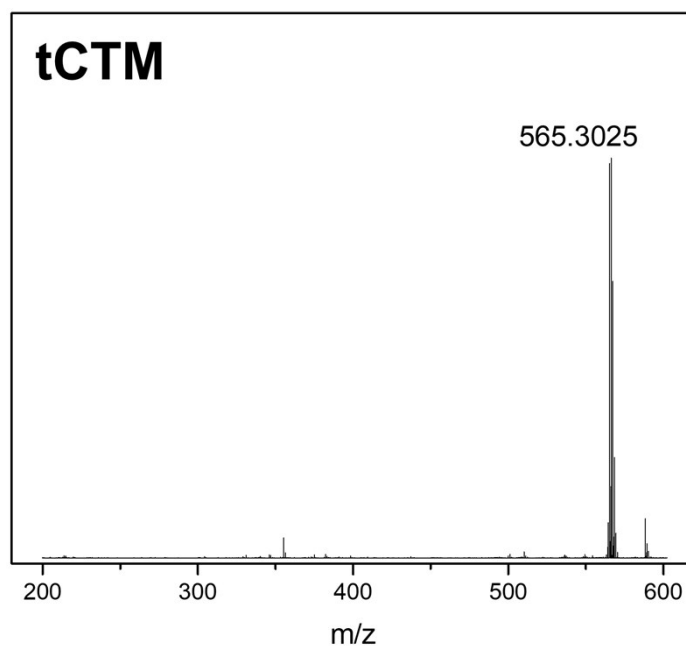**Fig. S23** MALDI-TOF-MS of compound **CTM**.

Fig. S24 MALDI-TOF-MS of compound **tCTM**.

3. References

1 H. Zhao, Z. Wang, X. Cai, K. Liu, Z. He, X. Liu, Y. Cao and S.-J. Su, *Mater. Chem. Front.*, 2017, **1**, 2039.

2 J. Guo, X.-L. Li, H. Nie, W. Luo, S. Gan, S. Hu, R. Hu, A. Qin, Z. Zhao, S.-J. Su and B. Z. Tang, *Adv. Funct. Mater.*, 2017, **27**, 1606458.

3 C. Lee, W. Yang and R. G. Parr, *Phys. Rev. B*, 1988, **37**, 785.

4 M. J. Frisch, G. W. Trucks, H. B. Schlegel, G. E. Scuseria, M. A. Robb, J. R. Cheeseman, G. Scalmani, V. Barone, G. A. Petersson, H. Nakatsuji, X. Li, M. Caricato, A. V. Marenich, J. Bloino, B. G. Janesko, R. Gomperts, B. Mennucci, H. P. Hratchian, J. V. Ortiz, A. F. Izmaylov, J. L. Sonnenberg, Williams, F. Ding, F. Lipparini, F. Egidi, J. Goings, B. Peng, A. Petrone, T. Henderson, D. Ranasinghe, V. G. Zakrzewski, J. Gao, N. Rega, G. Zheng, W. Liang, M. Hada, M. Ehara, K. Toyota, R. Fukuda, J. Hasegawa, M. Ishida, T. Nakajima, Y. Honda, O. Kitao, H. Nakai, T. Vreven, K. Throssell, J. A. Montgomery, Jr., J. E. Peralta, F. Ogliaro, M. J. Bearpark, J. J. Heyd, E. N. Brothers, K. N. Kudin, V. N. Staroverov, T. A. Keith, R. Kobayashi, J. Normand, K. Raghavachari, A. P. Rendell, J. C. Burant, S. S. Iyengar, J. Tomasi, M. Cossi, J. M. Millam, M. Klene, C. Adamo, R. Cammi, J. W. Ochterski, R. L. Martin, K. Morokuma, O. Farkas, J. B. Foresman, D. J. Fox, Wallingford and CT, *Gaussian 09, Revision E.01*, 2016.

5 F. Neese, *WIREs. Comput. Mol. Sci.*, 2012, **2**, 73.